USM3D Simulations for Second Sonic Boom Workshop

Alaa Elmiligui[1] and Melissa B. Carter[2]
NASA Langley Research Center, Hampton VA 23681

Sudheer N. Nayani[3]
Analytical Services & Materials, Inc., Hampton, VA 23666

Susan Cliff [4]
NASA AMES Research Center, Moffett Field, CA 94040

and

Jason M. Pearl[5]
University of Vermont, Burlington, VT 05401, US

The NASA Tetrahedral Unstructured Software System with the USM3D flow solver was used to compute test cases for the Second AIAA Sonic Boom Prediction Workshop. The intent of this report is to document the USM3D results for SBPW2 test cases. The test cases included an axisymmetric equivalent area body, a JAXA wing body, a NASA low boom supersonic configuration modeled with flow through nacelles and engine boundary conditions. All simulations were conducted for a free stream Mach number of 1.6, zero degrees angle of attack, and a Reynolds number of 5.7 million per meter. Simulations were conducted on tetrahedral grids provided by the workshop committee, as well as a family of grids generated by an in-house approach for sonic boom analyses known as BoomGrid using current best practices. The near-field pressure signatures were extracted and propagated to the ground with the atmospheric propagation code, sBOOM. The USM3D near-field pressure signatures, corresponding sBOOM ground signatures, and loudness levels on the ground are compared with mean values from other workshop participants.

I.   Introduction

The First Sonic Boom Prediction Workshop was held in January 2014 in conjunction with the AIAA Science and Technology Forum and Exposition (SciTech). A summary and statistical analysis of the First AIAA Sonic Boom Prediction Workshop (SBPW1) is given in Ref. [1-2]. The workshop focused on three configurations: an axisymmetric body with a flat-top ground signature, a simple nonlifting wing body with N-wave signature, and a complex configuration with wing, tail, flow-through nacelles, and blade mount sting (LM-1021). Details of all three configurations can be found in SBPW1 webpage, [3]. The main objective of the SBPW1 was to assess the state of the art of computational methods with international participation for predicting signatures suitable for sonic boom propagation. Impartial comparisons were made between different solution schemes as well as with wind tunnel validation data for assessing the state of the art and identifying areas requiring additional research and further development. The sonic boom workshop website has the listing of workshop participants and their presentations, [3]. A follow up special session was held at AIAA AVIATION Forum 2014 where presenters showed summary and analysis of SBPW1 test cases, Ref. [4-6].

In January 2017, the AIAA Applied Aerodynamics Technical Committee (APATC) conducted their 2nd Sonic Boom Workshop (SBPW2) during the AIAA Science and Technology Forum and Exposition (SciTech 2017) to build on the success of the SBPW1. The complexity of the models was increased slightly to include a configuration

---

[1]   Research Engineer, Configuration Aerodynamics Branch, Mail Stop 499, AIAA Senior Member.
[2]   Aerospace Engineer, Configuration Aerodynamics Branch, Mail Stop 499, AIAA. Associate Fellow
[3]   Senior Scientist, CFD Group, 107 Research Drive, AIAA Associate Fellow.
[4]   Aerospace Engineer, Applied Modeling and Simulations Branch, Moffett Field, AIAA Associate Fellow.
[5]   Graduate Student, College of Engineering and Mathematical Sciences, AIAA Student Member.

with powered engine jet effects, and the sonic boom loudness level of the configurations were lower than in the first workshop. The SBPW2 was a two-day event, the first day focused on near-field simulation and the second day included both near-field simulation and atmospheric propagation methods. The two-part workshop covered both the state-of-the-art for predicting near-field sonic boom signatures with CFD as well as propagation of the near-field pressures to the ground. The objectives of the workshop were to build on the success of the SBPW1; to assess the state-of-the-art computational methods as practical aerodynamics tools for predicting near filed pressure signatures for industry relevant geometries; and to identify areas needing additional research and development. The SBPW2 committee provided three required and one optional near-field CFD test cases. The test cases were an axisymmetric equivalent area body (AXIE), a JAXA wing body (JWB) [7], a NASA low boom supersonic configuration, C25D [8-9], with flow through nacelle (C25D-F) and with propulsive engine boundary conditions (C25D-P). The surface definition of all four test cases were designed to generate, at three body lengths, similar on-track near-field pressure signatures. A summary and statistical analysis of the SBPW2 participants' results are given in Reference 10.

In the present study, the NASA Tetrahedral Unstructured Software System (TetrUSS), Ref. [11], with its USM3D solver was used to compute flow fields for the SBPW2 test cases. The near-field pressure signatures were computed at distances of 1, 3, and 5 body lengths and at five off-track angles. The on-track and off-track signatures were propagated to the ground. All near-field pressure signatures, corresponding ground signatures, loudness levels, and aerodynamic force and moment computations were uploaded to the workshop website [3]. The near-field pressure signatures were propagated to the ground with the atmospheric propagation code, sBOOM, Ref. [12]. USM3D results are presented for both the workshop provided tetrahedral grids and on a second set of tetrahedral grids generated by "Boom Grid" (BG) grid generation methodology [13].

The organization of this paper will be as follows: (1) Description of the SBPW2 test cases; (2) Brief description of TetrUSS and USM3D; (3) Description of numerical grids used in the study; (4) Presentation of the numerical results and comparison with FUN3D and the SBPW2 participant's results; and (5) Conclusions.

II.   Sonic Boom Workshop Test Cases.

As previously mentioned, the four test cases were: an axisymmetric equivalent area body (AXIE), a JAXA Wing Body (JWB), a NASA low boom supersonic configuration with flow through nacelle (C25D-F), and with engine powered boundary conditions (C25D-P). Figure 1 shows a schematic of the SBPW2 test case configurations. The axisymmetric equivalent area body shown in Figure 1a was designed with Cart3D to match the near-field pressure signature of the inviscid NASA Concept 25D with a flow through nacelle at 3 body lengths on the centerline, Ref. [3]. JAXA provided the second test configuration, (JWB), Ref. [7], which was based on an inverse design to recover C25D equivalent area. A schematic of the JWB is shown in Figure 1b. The length of the JWB model was 38.7 m with a full span reference area of 65.6 m^2. The design angle of attack of 2.3° was included in the provided geometry. The third configuration was the NASA C25D-F with a flow through nacelle. The C25D is a conceptual low boom shape, demonstrator-class vehicle, designed at the NASA Langley Research Center, Ref. [8-9], and is shown in Figure 1c. The provided geometry included a rotation about the nose of 3.37° to pitch the model at the design angle of attack. The C25D has a length of 38.7 m and a reference area of 9.29 m^2. The fourth configuration was the NASA Concept 25D but with powered boundary conditions (C25D-P). All four test cases used at Mach number of 1.6 and an altitude of 15,760 m.

III.   Computational Technique

In this section, the details of the numerical approach and the computational grids used by USM3D to compute the flow field for the SBPW2 test cases are presented. USM3D is the flow solver used within TetrUSS, Ref. [14] that was developed at the NASA Langley Research Center (LaRC). TetrUSS includes a model/surface grid preparation tool (GridTool) [15], field grid generation software (VGRID), Ref. [16-17], and USM3D [14]. USM3D has internal software to calculate forces and moments, and additional post processing is accomplished with, the NASA LaRC-developed code USMC6, which was used for extracting off-body planes and cylinders as well as a specialized selection of on-body components for detailed analyses of the solutions. The atmospheric propagation code, sBOOM [12], has been selected to propagate USM3D near-field signatures to the ground.

A. USM3D Flow Solver

USM3D is an unstructured tetrahedral, cell-centered, finite volume, Euler, and Navier–Stokes flow solver. Time integration follows the implicit point Gauss–Seidel algorithm, explicit Runge–Kutta approach, and local time stepping for convergence acceleration. The solver scheme allows various options for computing the inviscid-flux quantities across each cell face. The Harten, Lax, and van Leer with contact restoration scheme (HLLC) [18] was

American Institute of Aeronautics and Astronautics

used for the inviscid flux discretization and the min-mod flux limiter have been used to smooth out the flow discontinuities due to shock waves. The Spalart Allmaras, one-equation turbulence model was used to model turbulence, Ref. [19].

B. sBOOM, Ground Propagation Code.

The NASA LaRC developed sonic boom prediction code, sBOOM, was used to propagate sonic boom signatures to the ground. sBOOM solves the augmented Burgers' equation numerically and takes into account effects such as nonlinearity, molecular relaxation and thermo-viscous absorption into the propagation process. The thickness of the shocks is predicted analytically, which avoids artificial smoothing and empirical shock thickening during loudness calculation. sBOOM can predict on-track and off-track ground signatures with or without wind effects, along with consideration for aircraft maneuvers. Further details about sBOOM and its applications can be found in reference [12]. The Loudness levels at the ground were computed by the code based on the procedure developed by Shepherd and Sullivan, Ref. [20].

C. Computational Grids

Two sets of grids were used in this study. The first set of grids was the tetrahedral grids provided by the SBPW2. The second set of grids was the in-house family of grids generated by VGRID for the inner grid and BG for the outer collar grid. The SBPW2 tetrahedral grids were a subdivision of the SBPW2 mixed-element grids. The SBPW2 grids were in full-scale meters and intended for a free-stream Mach number of 1.6 and zero degrees angle of attack. This section describes the details of the different grids.

SBPW2 Tetrahedral Grids

For the AXIE case, the SBPW2 provided five purely-tetrahedral inviscid grids. The grid size varied from 3.7 million tetrahedral cells on the coarsest grid to 332.1 million on the finest grid level. USM3D solutions were provided on all five grid levels. For the JWB case, the SBPW2 provided three purely-tetrahedral inviscid grids. The JWB grids have a uniformly refined spacing in all three dimensions with a scale factor of 0.70, 0.83, and 1.00. The coarse grid had 37.4 million tetrahedral cells and the finest grid had 109.1 million cells.

For the C25D-F case, the SBPW2 provided six inviscid grid levels but only the first five grid levels were used in the current study. The SBPW2 provided C25D grids that are purely-tetrahedral inviscid grids with a uniformly refined spacing in three dimensions. The coarse grid had 20.0 million cells while the finest inviscid grid used in this study had 305.2 million cells. The SBPW2 provided six viscous C25D grids, and only the coarsest grid level was used in this study. The C25D geometry included a rotation about the nose of 3.375° to pitch the model at the design angle of attack, and so the flow solver was run at zero degrees angle of attack.

The C25D-P was the fourth test case and it had the same surface definition as the third test case except that it had a powered boundary condition instead of a flow through nacelle. Similar to the C25D-F, the C25D-P had a body length equal to 32.92 m and a reference area of 9.29 m^2. Both inviscid and viscous grids were provided. Five inviscid grids were provided by the SBPW2 committee but only the first two grid levels were used in the current study. For the viscous grids, only the SBPW2 coarse grid was used. The reason for not running all of the SBPW2 tetrahedral grids was that the SBPW2 USM3D grids had collapsed cells with negative volumes. This problem was only in the cogsg grid file format used by USM3D, and did not show in any other C25D grid format. The cogsg grids were converted from ugrid format to cogsg format, Ref. [3]. In some of the test cases, the conversion resulted in negative volume tetrahedra cells in the cogsg format grid, which prevented USM3D from running the cases. The problem with the converter could not be resolved in time for the workshop, but an effort is underway to resolve this issue. To circumvent this issue in a timely manner and allow for USM3D to evaluate the C25D test case, a series of in-house grids were generated. Details of the SBPW2 grids are given in Table 1.

In-house SBPW2 Tetrahedral Grids

The NASA Tetrahedral Unstructured Software System grid generation tools were utilized to generate a set of in-house grids for the SBPW2 test cases. The TetrUSS grid generation package includes a geometry setup tool called Gridtool, Ref. [15], an unstructured grid generation program called VGRID, Ref. [16-17] and a postprocessor named POSTGRID. The computer-aided design (CAD) model of the configuration, typically an IGES file, is read into the preprocessing code GridTool where the curves, patches on the surfaces, and far-field are defined. The grid generation requires two steps. In the first step, VGRID was used to generate a refined near-field grid with a cylindrically shaped boundary that encompasses the model just beyond its surface. In the second step, the Boom Grid (BG) method is used to generate the outer collar grid where tetrahedral cells are aligned to the freestream Mach angle. More details about grid generation for supersonic boom calculations can be found in Ref. [13]. In this section, a brief description of VGRID and BG are provided.

Table 1. SBPW2 Grid Details.

Test Case	Grid Type	Grid Name	Scale Factor	Nodes	Tetrahedral Cells
AXIE	Inviscid	AXIE_1	2.56	646,467	3,705,046
	Inviscid	AXIE_2	2.00	1,601,681	9,243,626
	Inviscid	AXIE_3	1.60	5,077,104	29,682,640
	Inviscid	AXIE_4	1.28	15,911,412	93,751,314
	Inviscid	AXIE_5	61.00	56,085,031	332,136,840
JWB	Inviscid	JWB-1	1.00	6,491,425	37,397,159
	Inviscid	JWB-2	0.83	11,335,260	65,432,421
	Inviscid	JWB-3	0.70	18,875,613	109,141,197
C25D	Inviscid	C25D-F1	2.00	3,419,776	19,995,530
	Inviscid	C25D-F2	1.60	6,323,343	37,082,947
	Inviscid	C25D-F3	1.28	13,083,168	77,082,860
	Inviscid	C25D-F4	1.00	26,923,206	159,106,053
	Inviscid	C25D-F5	0.80	51,542,500	305,204,267
	Viscous	C25D-FV1	2.00	4,789,378	28,090,664
C25D-P	Inviscid	C25D-P1	2.00	3,421,840	19,987,689
	Inviscid	C25D-P2	1.60	6,393,433	37,486,198
	Viscous	C25D-PV1	2.00	4,856,211	28,470,874

VGRID is a tetrahedral unstructured grid generation program that can be run interactively or in batch mode. VGRID can produce grids suitable for computing Euler or Navier-Stokes flow solutions and uses the Advancing-Layers method (ALM) and the Advancing-Front method (AFM), Ref. [16-17] to generate volume grid. Both techniques are based on marching processes in which tetrahedral cells are grown on an initial triangular boundary mesh and gradually form in the field around the geometry. Once the advancing front process is completed in VGRID, an additional post-processing step is required using POSTGRID to close any open pockets in the grid and improve grid quality. The current version of VGRID includes growth rates, surface sources, and volume sources. The grid spacing is related to the strength of user-defined sources placed in the domain. The user-defined sources can be point, line or volume sources. Volume sourcing can be a sphere, a cylinder, or a cone. The guidelines established by the Drag Prediction Workshop, Ref. [21], and the High Lift Prediction Workshop, Ref. [22], were adopted in the grid generation process. For the current set of grids, the inner grid outer boundary was at 0.02*body lengths from the wing tip. The boundary layer growth rate was governed by following equation:

$$\delta_j = \delta_1 * (1 + R_1*(1 + R_2)^{j-1,j-1})$$

where δ_1 is the first cell height and rate1 (R_1) and rate2 (R_2) are 0.15 and 0.05, respectively.

The BG method was used to generate outer collar grids. BG is similar to other "extrusion" grid generation approaches, Ref. [13], in that the new grid is created by extending lines from grid points on a boundary surface for an existing grid in the direction of the Mach cone angle for the applicable Mach number that the desired solution is to be obtained. The new cells are extruded through the outer, typically cylindrical, far-field boundary of the existing "core" 3-D grid around a configuration, creating a "collar" grid. The extension direction is approximately normal to the original surface points when viewed from the front, but the new grid lines are swept in the streamwise direction to the Mach angle. This grid line shearing, along with stretching of the distance between subsequent layers, creates high-aspect ratio cell faces that are closely aligned with the Mach angle so that the dissipation of the boom signature is reduced. Depending on the desired location for extracting a sonic boom signature, anywhere from 20 to more than 100 layers of cells may need to be generated. The BG grids were used to compute the on-track near-field signatures. Details of BG grids used in the current study are given in Table 2.

Table 2 Detail of in-house tetrahedral grids for SBPW2 test cases

Test Case	Grid Type	Grid Name	Nodes	Tetrahedral Cells
AXIE	Inviscid	VGRID_1	646,467	47,821,570
	Inviscid	VGRID_2	15,918,977	93,341,956
	Inviscid	VGRID_3	49,670,934	293,292,643
JWB	Inviscid	VGRID_1	2,288,839	13,242,743
	Inviscid	VGRID_2	4,469,805	25,999,618
	Inviscid	VGRID_3	7,228,240	42,220,169
C25D	Viscous	VGRID_1	11,213,517	65,707,776
	Viscous	VGRID_2	22,429,694	131,941,166
	Viscous	VGRID_3	63,040,357	372,736,328
C25D-P	Viscous	VGRID_1	7,032,725	40,697,679
	Viscous	VGRID_2	10,475,401	60,769,047
	Viscous	VGRID_3	26,813,151	157,470,188

D. Boundary Conditions

For the inviscid flow simulations, a tangent flow aerodynamic surface boundary condition was used on all solid surfaces. The supersonic inflow boundary condition was used at the domain inflow face and the extrapolation boundary condition was used at the downstream outflow face of the domain. The characteristic inflow and outflow boundary condition was used along the far field, lateral faces of the outer domain. For viscous simulations, the no-slip viscous boundary condition was used on all solid surfaces. For the C25D-P configuration, USM3D jet boundary conditions were used to simulate the powered engine. In USM3D, the jet boundary condition requires only the values for total pressure, $P0jet$, and total temperature, $T0jet$, at the engine exhaust face. The inlet-plane flow is determined automatically through a mass flux balance with the jet and fan flows by adjusting an average back pressure on the face. By using an average back pressure, any distortion on the inflow plane is maintained while the mass flux is balanced.

IV. Results and Discussion

USM3D results for SBPW2 test cases will be presented and discussed in this section. The simulations were performed for a free stream Mach number of 1.6, zero degrees angle of attack, and Reynolds number equal to 5.70 million per meter for the optional viscous simulation. The surface definitions had the design angle of attack built into the geometry. For each configuration, the near-field pressure signatures were extracted at distances of 1, 3, and 5 body lengths away from surface. The near-field pressure signatures were extracted at off-track angles, φ, of 0°, 10°, 20°, 30°, 40° and 50°. The near-field on-track and off-track signatures were extracted from UMS3D simulation solution files using USMC6; propagated to the ground using SBOOM; and the sound levels at the ground were computed with Loudness code, Ref. [20]. All the near-field signatures, propagated ground signatures and corresponding loudness levels were uploaded to the workshop website, Ref. [3]. In this paper, only the near-field pressure signatures at a distance of 3 body lengths away from surface will be presented.

The Axisymmetric Equivalent Area Test Case (AXIE):

USM3D inviscid simulations were conducted for the AXIE Case on both SBPW2 grids and on the in-house BG grids. Figure 2 shows the AXIE symmetry plane colored with USM3D pressure coefficient contours on the SPWP2 provided fine grid. The black horizontal line near the bottom of the figure depicts the location of the extracted pressure signature at three body lengths below the configuration. Figure 3 shows the symmetry plane colored by the density gradient. Lines of constant density gradient extend to the far boundary, and shock and expansion regions of the flow field slowly decay; these are qualitative indications that the USM3D solver, on the provided grids, captures the sonic boom signature to the far-field boundary. Figure 4 shows the USM3D near-field pressure signatures extracted from the SBPW2 tetrahedral grids at three body lengths. The near-field pressure signatures on the two coarsest grids, AXIE-1 and AXIE-2, are not grid converged, however, the solution is grid converged on the finer grids. Figure 5 shows the comparison of USM3D, FUN3D, and workshop mean near-field pressure signatures. The USM3D results, both on the workshop provided grids and on the BG grid, are in excellent agreement with FUN3D

results. This was expected since both USM3D and FUN3D used the same workshop provided tetrahedral-celled grids. However, it is noted that USM3D is a cell centered code while FUN3D is a node based code.

Each of the near-field pressure signatures were propagated to the ground using sBOOM starting from a cruise altitude of 15,760 m and at an off-body distance of one, three and five body lengths away from body. The corresponding ground loudness levels were also computed. Figure 6 shows the comparison of the ground signatures for the near-field pressure signatures extracted from a distance of 3 body lengths away from surface. The comparison between predictions visually looks good in the front portion of the signature and it slightly differs in the aft part of the signature. The difference in perceived loudness level between signatures shown in Figure 6 is less than 0.8 dB. The corresponding loudness levels are shown in the legend of Figure 6.

The JAXA Wing Body Test Case (JWB)

JAXA provided the surface definition for the second workshop test case configuration, the JAXA Wing Body. The surface definition was based on an inverse design to recover the equivalent area of the C25D. A schematic of the JWB is shown in Figure 1b. Inviscid simulations were conducted for JWB test case on both SBPW2 grids and BG grids. Figure 7 shows contours of overpressure at three body lengths away from body. The black lines depict the location of the extracted pressure signatures at 3 body length away from JWB. Figure 8 shows USM3D off-track near-field pressure signatures extracted on the JWB_3 grid at three body lengths. As expected, larger expansions in the aft portion of the signatures are encountered as we move away from the symmetry plane (direction of increasing phi). This can be shown at an X location of ~ 158 m in Figure 8 and can also be visualized by the increase in red color contour in Figure 7. Figure 9 shows a comparison of the USM3D on-track near-field pressure signatures with FUN3D, and the workshop mean near-field pressure signatures at three body lengths. The comparison between predictions is considerably better, visually, in the front portion and deteriorates in the aft part of the signature. The USM3D solution on JWB_3 does not accurately capture the magnitude of the compression and expansion waves; predictions are washed out due to the nature of the grid. USM3D predictions with VGRID_3 is more aligned with FUN3D and with the participants mean predictions. The USM3D front portion of the signatures, on VGRID_3, correlates well with other codes, however, the correlation worsens in the aft portion yielding much stronger shocks than the other computations or the mean of the workshop participants signatures.

JWB near-field pressure signatures were propagated to the ground using sBOOM assuming a cruise altitude of 15,760 m. The corresponding ground loudness levels were also computed. Figure 10 shows the comparison of the ground signatures for the propagated near-field pressure signatures extracted from a distance of 3 body lengths away from surface. The comparison between predictions looks visually good in the front portion of the signatures and deteriorates in the aft portion. All four-ground signatures have approximately the same wavelength. The corresponding loudness levels are shown in the legend of Figure 10. The peak of the ground signatures varied by less than 0.03 psf. The difference in perceived loudness levels between signatures shown in Figure 10 is less than 3 dB, however, if the USM3D simulation on the JWB-3 grid is ignored, the difference in perceived loudness level between signatures will be less than 1 dB.

NASA Concept 25D with Flow Through Nacelle (C25D-F).

The C25D is a NASA conceptual low boom shape demonstrator-class vehicle designed at the NASA Langley Research Center. The C25D concept was shown in Figure 1c. USM3D inviscid as well as viscous simulations were conducted for C25D-F with flow through nacelles. The SBPW2 committee provided six inviscid and six viscous purely-tetrahedral grids. USM3D computations were conducted on the five coarsest inviscid grids and on the coarsest viscous grid. The simulations were not performed on the other grids because the provided grids had collapsed cells. USM3D simulations were also conducted on three in-house BG viscous grids. Details of the grids were given in Tables 1 and 2.

Figure 11 shows USM3D inviscid overpressure contours at one, three, and five body lengths away from the body. The black lines depict the locations of the extracted pressure signatures. Figure 12 shows the symmetry plane colored by the density gradient contours. The density gradient lines below the configuration extend parallel to the free stream Mach cone angle and show a benign region in the flow field. On the other hand, the complexity of the flow field is clearly visible at the aft part of C25D configuration where shock and expansion waves emanating from the C25D tail interact with the flow passing through the nacelle. Figure 13 shows USM3D inviscid on-track overpressure signatures, computed on the SBPW2 grids, at three body lengths away from C25D configuration. Figure 13 visually shows that the predicted signatures from the two finest grid levels, black and orange lines, are grid converged. The propagated ground signatures, shown in Figure 14, also show that the signatures are grid converged. The difference in loudness levels between the two finest grid levels is less than 0.15 dB. The front

portion of the ground signatures, up to a time of 60 ms are in good agreement while the comparison worsens in the aft part of the signatures. The main discrepancies appear between times of 70 and 90 ms.

Figure 15 shows comparison of C25D-F near-field viscous pressure signatures. Figure 15 shows that USM3D signatures are grid converged and compares well with FUN3D results. Slight discrepancy can be seen around $X \sim$ 154 m. USM3D viscous near-field signatures were propagated to the ground using sBOOM and the result is shown in Figure 16. Comparison is good between USM3D and FUN3D propagated signatures and the they fall within the standard deviation of the signatures submitted by SBPW2 participants. Slight differences can be seen around $\sim$ 70 ms.

NASA Concept 25D with Powered Engine (C25D-P).

The C25D-P test case is similar to the C25D except that C25D-P had a powered boundary condition instead of a flow through nacelle. In the current study, the engine plenum total pressure ratio to freestream static pressure was set to 14.54 and the engine plenum total temperature ratio to freestream static temperature was set to 7.87. Although the SBPW2 committee provided the engine fan face static pressure ratio to freestream static pressure, it was not utilized in the USM3D simulations. The engine inlet flow in USM3D is determined automatically through a mass flux balance with the jet and fan flows by adjusting an average back pressure on the face.

USM3D inviscid and viscous simulations were conducted only on the two coarsest SBPW2 inviscid and viscous grids, as the finest grid levels had negative volume tetrahedra. USM3D simulations were also conducted on three BG viscous grids. Details of the grids have been given in Tables 1 and 2. Figure 17 shows contours of overpressure differences at one, three, and five body lengths away from C25D-P. The black lines depict the location of the extracted pressure signatures. The attenuation of overpressure is apparent with increasing distance from the C25D-P configuration. Figure 18 shows the symmetry plane colored by the density gradient. The density gradient lines emanating from C25D-P configuration extend parallel to the Mach cone angle. The density gradient lines at the aft part of the configurations show a more complex flow field where shocks emanating from tail components interact with the plume flow. The complex flow features affect the overpressure field even at greater distances from the C25D-P configuration, thus making a full grid converged solution difficult to achieve. Figure 19 shows USM3D viscous on-track near-field pressure signatures, extracted from three body-lengths away form C25D-P. Figure 19 shows that the front portion of the signature is grid converged with signatures overlaying on each other, however, discrepancies can be viewed at the aft part of the signature at an X location of $\sim$ 158 m. These differences in overpressure trace back to the flow field at the back of the C25D-P configuration. The complex flow pattern at the aft part of C25D-P configuration results in small differences in overpressure where shocks emanating from the tail interact with the plume flow. Figure 20 shows a comparison between viscous simulations of USM3D, FUN3D, and the SBPW2 participants' mean near-field pressure signatures. The comparison looks good in the front part of the signature up to an X of $\sim$ 148 m. There is good agreement between all three signatures in predicting the shock and expansion locations. USM3D predicts stronger shocks while the flow expands more with FUN3D as can be seen at X of $\sim$ 154 m. Discrepancies can be observed in the signatures at an X location $\sim$ 158 m. Figure 21 shows the C25D-P ground signatures propagated from the USM3D viscous simulations. The front part of the ground signatures show that the front part of the signatures is grid converged while the aft part shows slight discrepancies. The difference in perceived loudness level between signatures extracted from coarse, medium and fine grids is $\sim$ 0.6 dB. The near-field pressure signatures of USM3D, FUN3D, and the SBPW2 participants mean were propagated to the ground with sBOOM and the corresponding ground signatures are shown in Figure 22. As expected, the comparison looks good in the front part of the signature while the aft part shows some discrepancies. The difference in perceived loudness level between signatures shown in Figure 22 is less than 0.8 dB. Results clearly show that realizing a grid converged solution in the front part of the signature has been achieved while the aft part remains a challenge that still needs to be addressed. This is true in all four test cases.

V. Conclusions

The SBPW2 test cases included an axisymmetric equivalent area body, a JAXA Wing Body, a NASA low boom supersonic configuration with flow through nacelles and with engine boundary conditions. USM3D simulations were conducted on all four test cases on the SBPW2 provided grids as well as BG grids. Near-field pressure signatures were analyzed at one, three and five body lengths away from the test configurations. The pressure signatures were evaluated at an off-track angle equal to 0°, 10°, 20°, 30°, 40° and 50°. The signatures were propagated to the ground with sBOOM and corresponding loudness levels computed. USM3D on-track results were compared with FUN3D and with mean values from SBPW2 participants.

For the AXIE case, the USM3D results were in excellent agreement with the FUN3D pressure signatures and within the bounds of the error estimate of the participants' results. The USM3D solution for the JWB on the JWB_3 grid didn't accurately capture the compression and expansion waves; the predictions were washed out due to nature of the grid. USM3D predictions for JWB on VGRID_3 grid was in better agreement with FUN3D and the mean predictions of participant's results. For the C25D, the comparison between USM3D, and FUN3D near-field pressure signatures as well as ground propagated signatures, were in good agreement. The signatures fall within bounds of error estimates of the participants' results. Small discrepancies can be observed in the aft part of the signatures that can be attributed to the complex flow region at the aft part of the C25D configuration. In summary, dense, stretched, and shock aligned grids are a key parameter in capturing the near-field pressure signatures. The impact of undershoots and overshoots, commonly present in near-field signatures, can be seen in the ground signatures. Results showed that slight variation in the magnitude and the location of the shocks and expansion waves can impact the loudness levels on the ground.

Acknowledgments

References

1. Michael A. Park and John M. Morgenstern. "Summary and Statistical Analysis of the First AIAA Sonic Boom Prediction Workshop", 32nd AIAA Applied Aerodynamics Conference, AIAA AVIATION Forum, (AIAA 2014-2006)
2. John M. Morgenstern. "Measurements Supporting 1st Sonic Boom Prediction Workshop Cases", 32nd AIAA Applied Aerodynamics Conference, AIAA AVIATION Forum, (AIAA 2014-2007).
3. AIAA Sonic Boom Prediction Workshop, Available: https://lbpw.larc.nasa.gov. [Accessed March 2017].
4. Aftosmis, M. J. and Nemec, M., "Cart3D Simulations for the First AIAA Sonic Boom Prediction Workshop", AIAA 2014–558, 2014.
5. Franck Dagrau, Adrien Loseille, and Itham Salah El Din. "Computational and Experimental Assessment of Models for the First AIAA Sonic Boom Prediction Workshop Using Adaptive High Fidelity CFD methods", 32nd AIAA Applied Aerodynamics Conference, AIAA AVIATION Forum, AIAA 2014-2009.
6. Jeffrey A. Housman, Emre Sozer, and Cetin C. Kiris. "LAVA Simulations for the First AIAA Sonic Boom Prediction Workshop", 32nd AIAA Applied Aerodynamics Conference, AIAA AVIATION Forum, AIAA 2014-2008.
7. Ueno, A., Kanamori, M., and Makino, Y., "Multi-fidelity Low-boom Design Based on Near-field Pressure Signature," AIAA Paper 2016–2033, 2016.
8. Mathias Wintzer and Irian Ordaz. "Under-Track CFD-Based Shape Optimization for a Low-Boom Demonstrator Concept", 33rd AIAA Applied Aerodynamics Conference, AIAA AVIATION Forum, AIAA 2015-2260.
9. Irian Ordaz, Mathias Wintzer, and Sriram K. Rallabhandi. "Full-Carpet Design of a Low-Boom Demonstrator Concept", 33rd AIAA Applied Aerodynamics Conference, AIAA AVIATION Forum, AIAA 2015-2261.
10. Michael A. Park, and Marian Nemec, "Nearfield Summary and Statistical Analysis of the Second AIAA Sonic Boom Prediction Workshop" To be published in AIAA Aviation 2017 Forum, Denver, CO.
11. Frink,N.T., Pirzadeh, S.Z, Parikh, P.C., Pandya, M.J., and Bhat, M.K., "The NASA Tetrahedral Unstructured Software System", The Aeronautical Journal, Vol. 104, No. 1040, October 2000, pp. 491-499. [1]
12. Sriram K. Rallabhandi. "Advanced Sonic Boom Prediction Using the Augmented Burgers Equation", Journal of Aircraft, Vol. 48, No. 4 (2011), pp. 1245-1253.
13. Michael A. Park, Richard L. Campbell, Alaa A. Elmiligui, Susan E. Cliff, and Sudheer Nayani. "Specialized CFD Grid Generation Methods for Near-Field Sonic Boom Prediction", 52nd Aerospace Sciences Meeting, AIAA SciTech Forum, AIAA 2014-0115.
14. Abdol-Hamid, K. S., Frink, N. T., Deere, K. A., and Pandya, M. J.: "Propulsion Simulations Using Advanced Turbulence Models with the Unstructured-Grid CFD Tool, TetrUSS", AIAA 2004-0714, January 2004.
15. Samareh, J. A.: "GridTool: A Surface Modeling and Grid Generation Tool", Proceedings of the Workshop on Surface Modeling, Grid Generation, and Related Issues in CFD Solutions, NASA Lewis Research Center, Cleveland, OH, NASA CP-3291, 1995, May 9-11, 1995.
16. Pirzadeh S., "Advanced Unstructured Grid Generation for Challenging Aerodynamics Applications." AIAA-2008-7178.
17. Kania, L. and Pirzadeh, S. Z., "A Geometrically-Derived Background Function for Automated Unstructured Mesh Generation", AIAA 2005-5240.
18. Harten, A., Lax, P. D., and van Leer, B., "On Upstream Differencing and Godunov-Type Scheme for Hyperbolic Conservation Laws," SIAM Review, Vol. 25, No. 1, 1983, p. 35.
19. Spalart, P.; and Allmaras, S.A., "One-equation turbulence model for aerodynamic flows." AIAA 92-0439, January 1992.

20. K.P. Shepherd and B.M. Sullivan. "A loudness calculation procedure applied to shaped sonic booms" NASA-TP-3134. 1991.
21. 6th AIAA CFD Drag Prediction Workshop. Available: https://aiaa-dpw.larc.nasa.gov/. [Accessed 10 April 2017]
22. 2nd AIAA CFD High Lift Prediction Workshop (HiLiftPW-2). Available: https://hiliftpw.larc.nasa.gov/index-workshop2.html. [Accessed 10 April 2017].
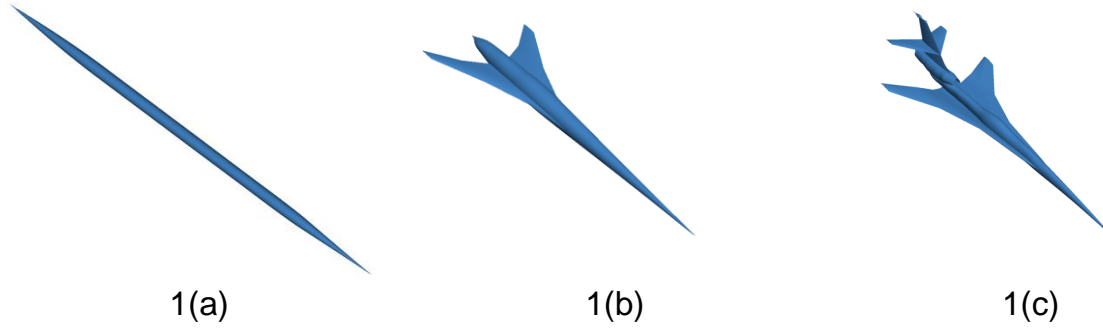
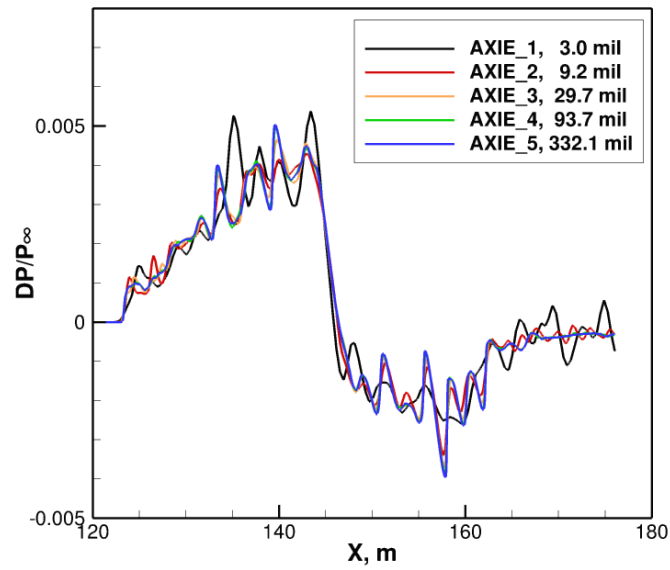**Figure 1. Schematic of the Sonic Boom Prediction Workshop test cases.**
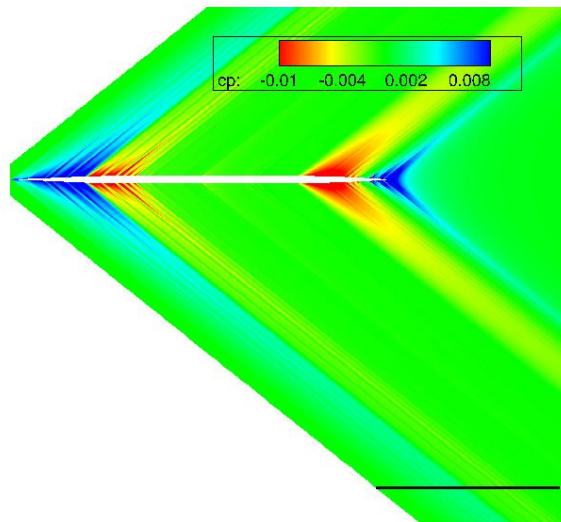
Figure 2. Symmetry Plane colored by coefficient of pressure, Cp, contours.
USM3D solution of the AXIE configuration, M$_\infty$=1.6, α=0.0º.

9
American Institute of Aeronautics and Astronautics
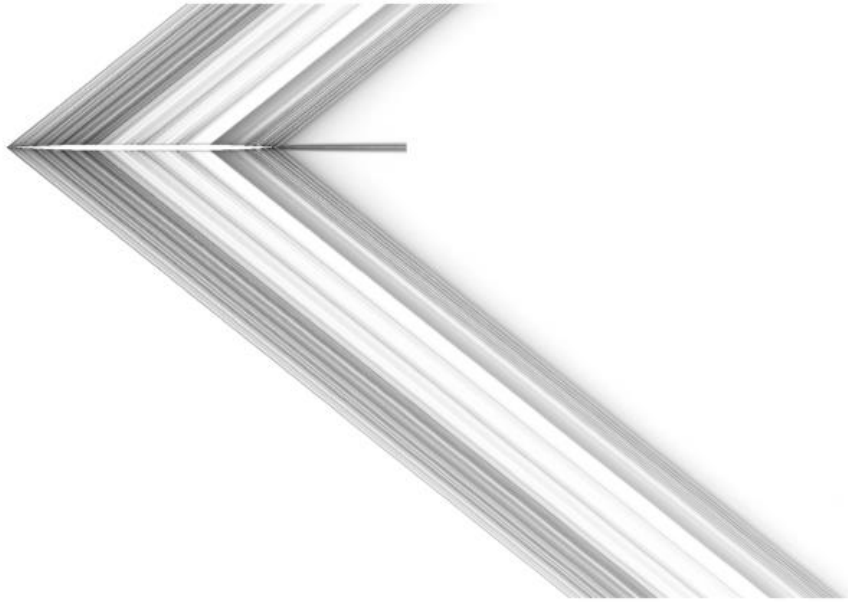
Figure 3. Symmetry plane colored by density gradient contours.
USM3D solution of the AXIE configuration, M_∞=1.6, α=0.0º.

Figure 4. USM3D near-field pressure signatures on SBPW2 grids.
USM3D solution for the AXIE configuration, M_∞=1.6, α=0.0º.

American Institute of Aeronautics and Astronautics
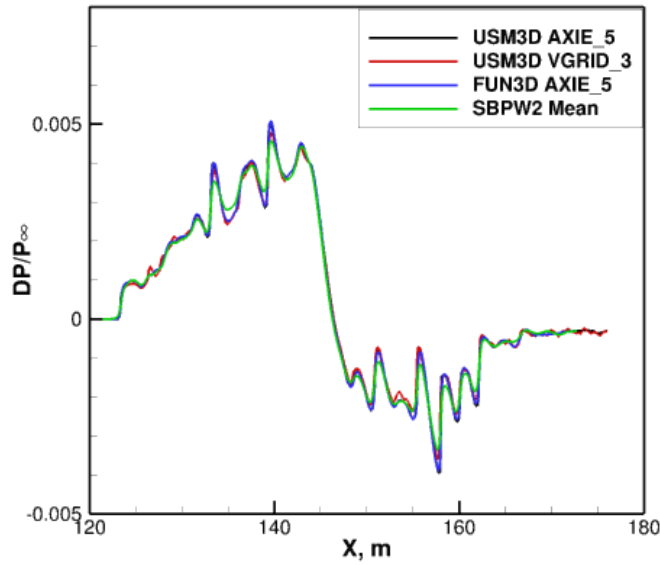
Figure 5. Comparison of near-field pressure signatures for AXIE configuration.
M_∞=1.6, α=0.0°.
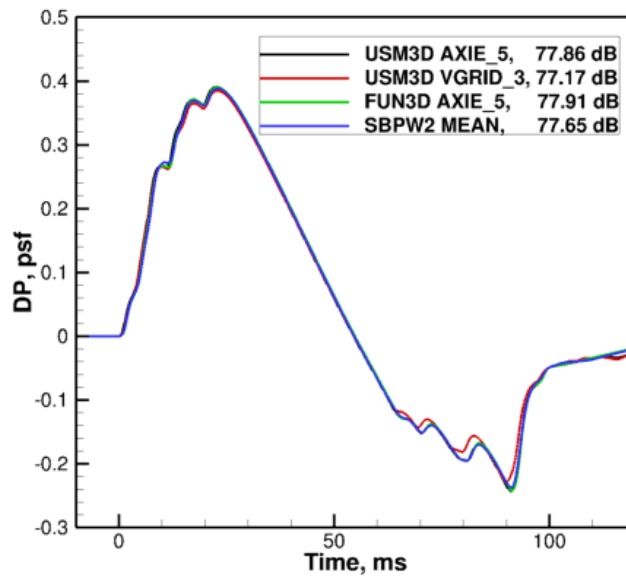
Figure 6. Comparison of sBOOM ground signatures of the AXIE configuration.
M_∞=1.6, α=0.0°.

American Institute of Aeronautics and Astronautics
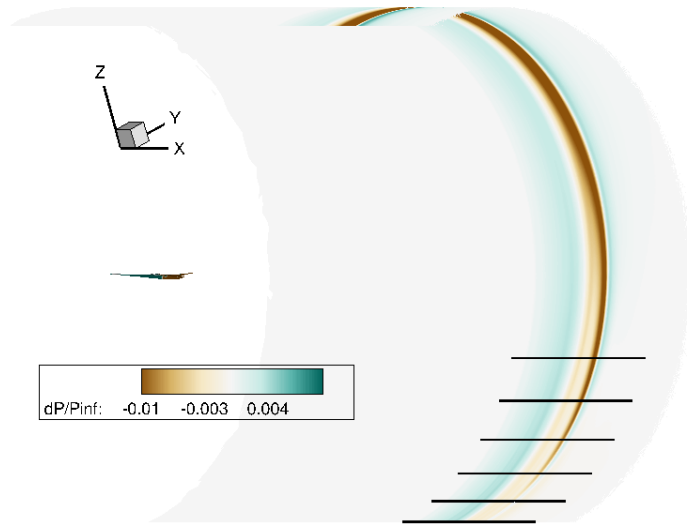
Figure 7. USM3D computed overpressure contours of the JWB at three body length away from body. Black horizontal lines show the near-field pressure data extraction locations. M_∞=1.6, α=0.0°.
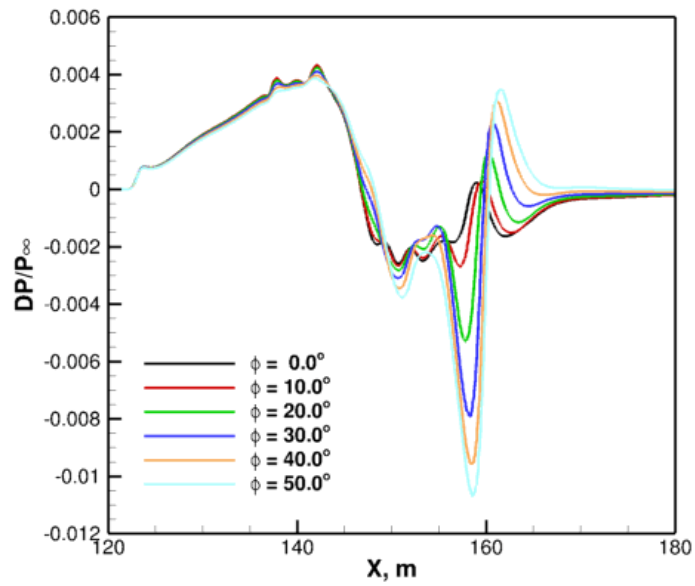
Figure 8. USM3D off-track near-field pressure signatures on the JWB_3 grid. M_∞=1.6, α=0.0°.
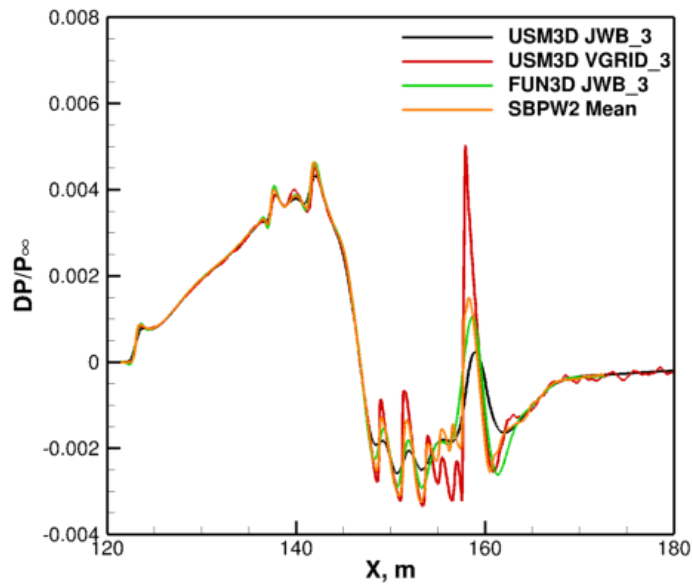
Figure 9. Comparison of near-field pressure signatures for JWB configuration. M_∞=1.6, α=0.0°.
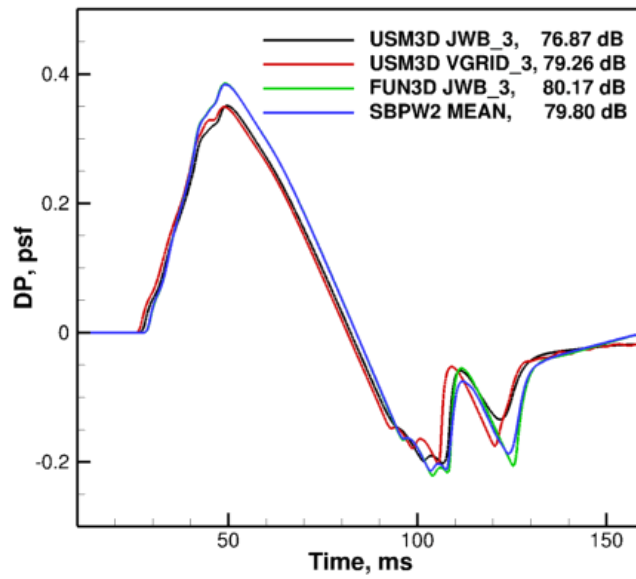
Figure 10. Comparison of sBOOM ground signatures of the JWB configuration. M_∞=1.6, α=0.0°.

American Institute of Aeronautics and Astronautics
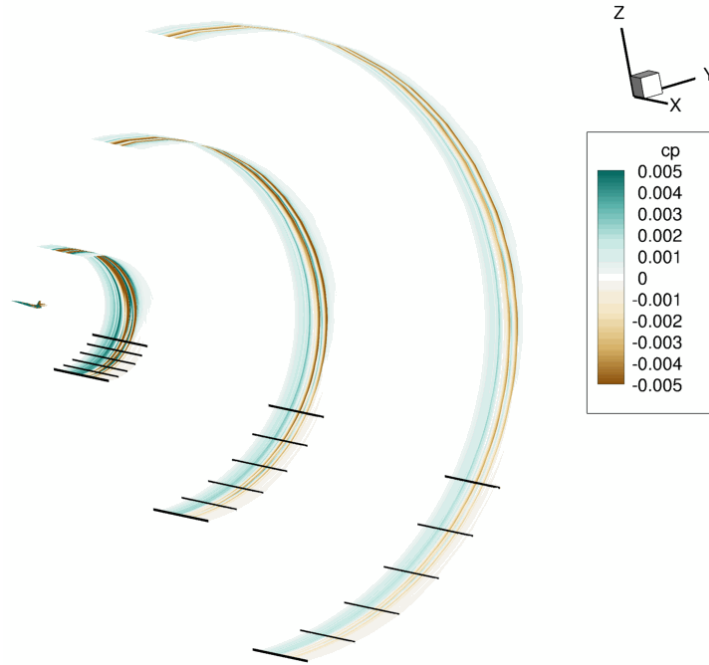
Figure 11. C25D USM3D inviscid overpressure contours.
Black lines show the near-field pressure data extraction locations at distances of 1, 3, and 5 body lengths away from C25D. M$_\infty$=1.6, α=0.0º.
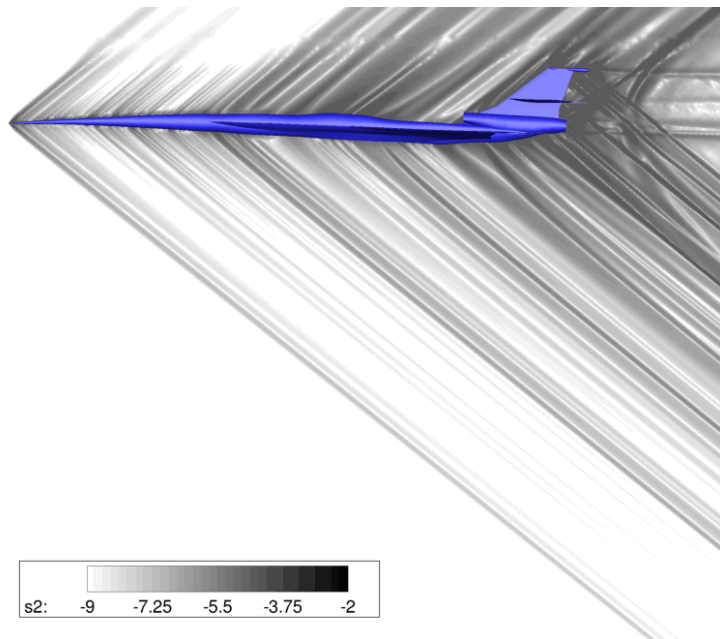
Figure 12. C25D symmetry plane colored by USM3D density gradient contours. M$_\infty$=1.6, α=0.0º.
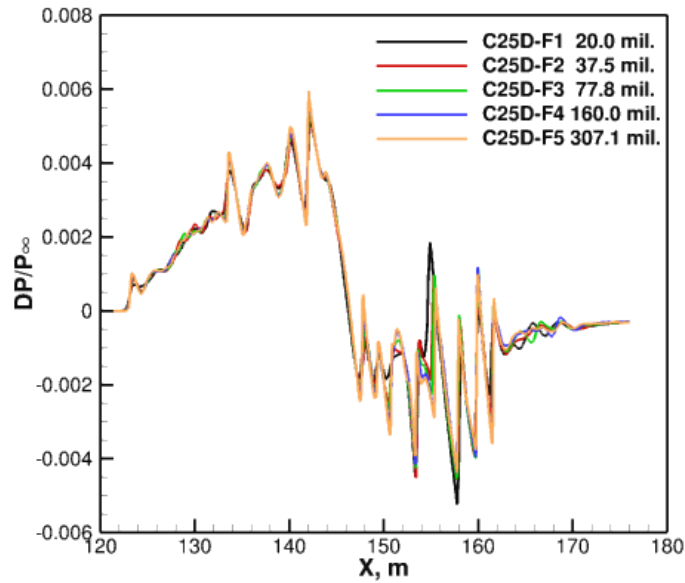
Figure 13. USM3D inviscid near-field pressure signatures on C25D flow through grids. M∞=1.6, α=0.0º.
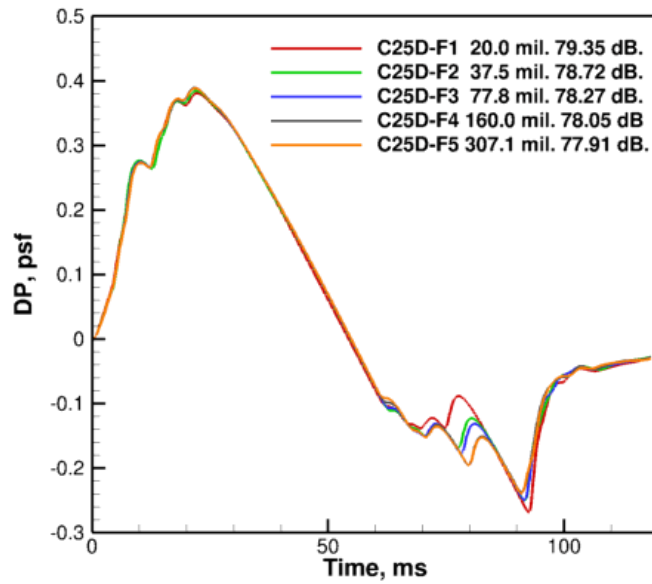
Figure 14. Comparison of ground signatures for C25D USM3D inviscid simulations on SBPW2 tetrahedral grids. Propagated near-field ground signatures extracted at three body length away from body. M∞=1.6, α=0.0º.
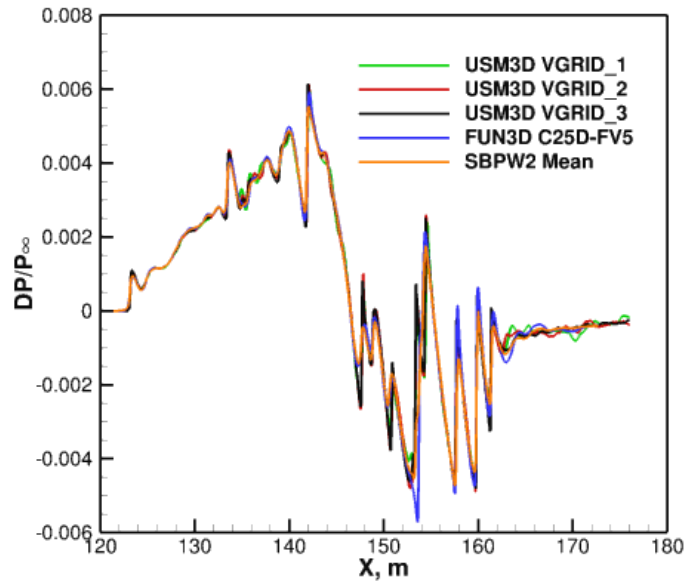
Figure 15. Comparison of near-field pressure signatures for C25D viscous simulations.
M_∞=1.6, α=0.0°, Rn=5.7 million per meter.
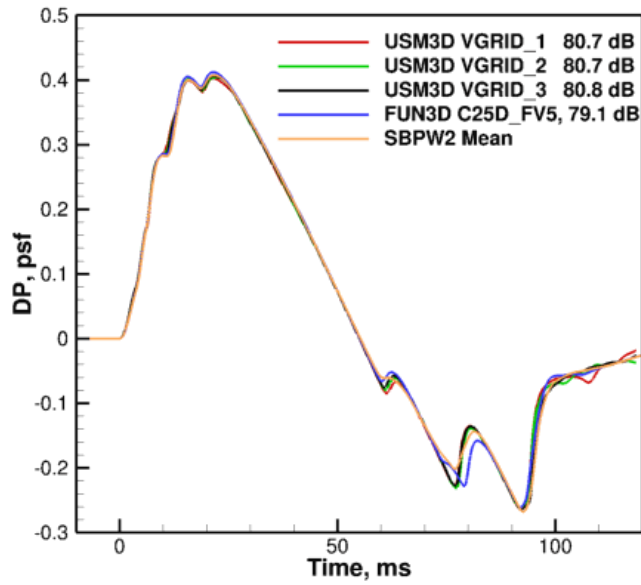
Figure 16. Comparison of ground signatures for C25D viscous simulations.
Propagated near-field ground signatures extracted at H/L=3, M_∞=1.6, α=0.0°, Rn=5.7 million per meter.

American Institute of Aeronautics and Astronautics
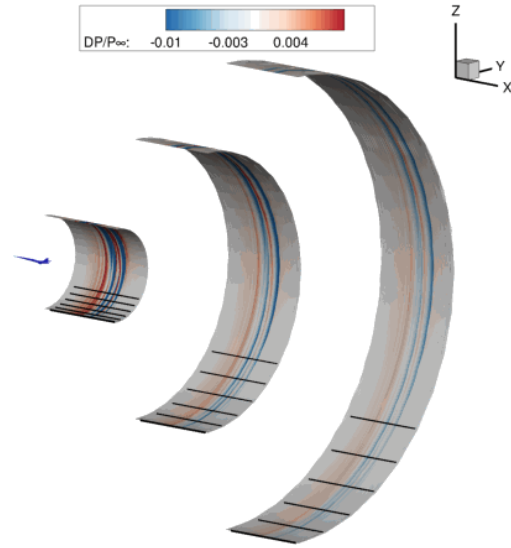
Figure 17. C25D-P USM3D overpressure, DP/P$_\infty$, contours at distances of 1, 3, and 5 body lengths away from C25D. M$_\infty$=1.6, α=0.0º, Rn=5.7 million per meter.
Black lines show the near-field pressure data extraction locations.
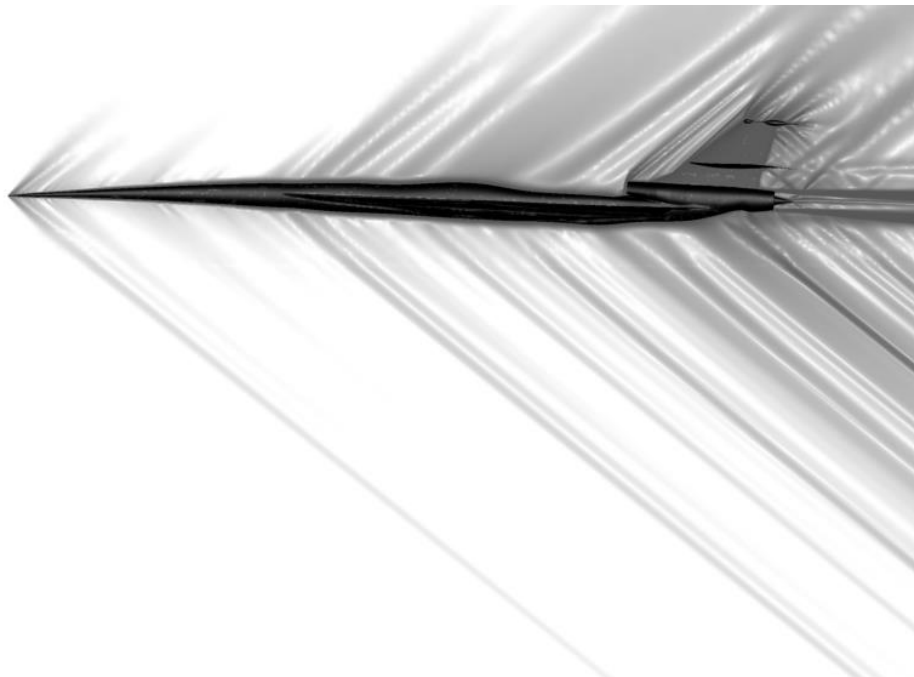
Figure 18. C25D-P USM3D symmetry plane density gradient contours.
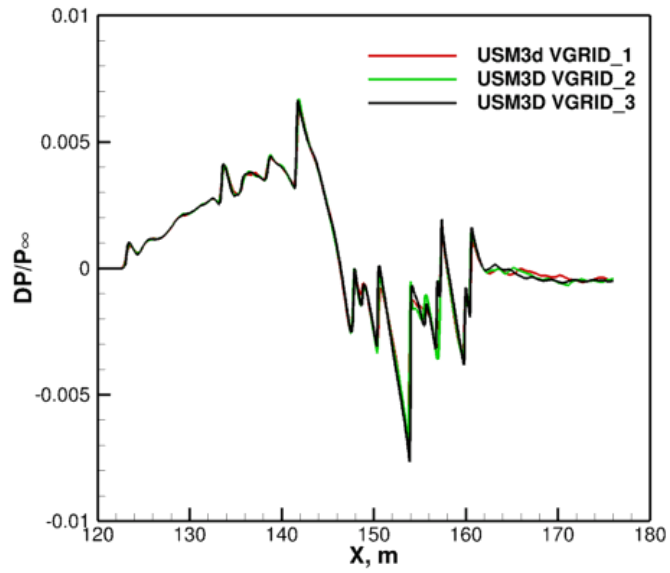**M$_\infty$=1.6, α=0.0º, Rn=5.7 million per meter.**

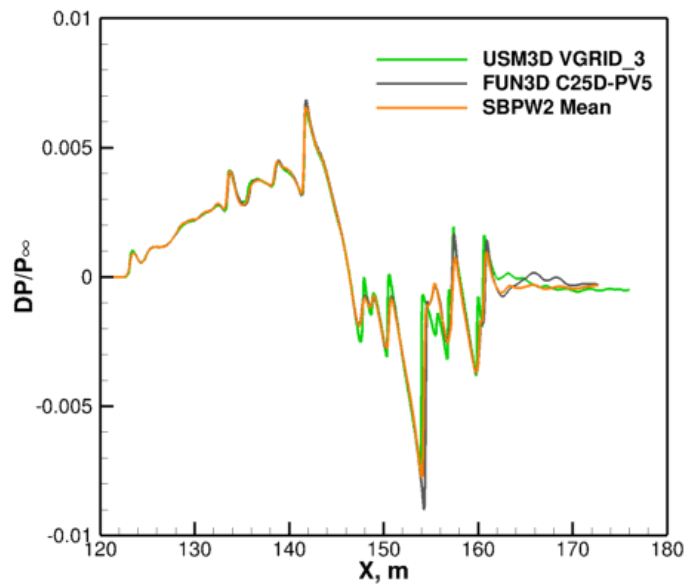**Figure 19. C25D-P USM3D viscous near-field pressure signatures at 3 body lengths away from C25D. M∞=1.6, α=0.0º, Rn=5.7 million per meter.**

Figure 20. Comparison of near-field pressure signatures at 3 body lengths away from C25D. M∞=1.6, α=0.0º, Rn=5.7 million per meter.
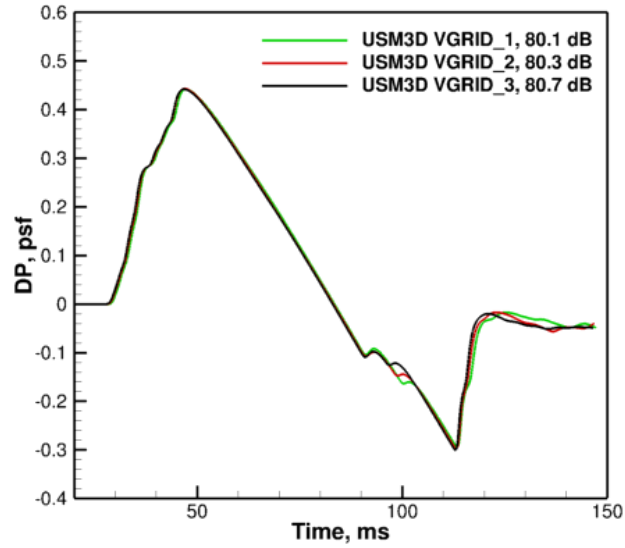
Figure 21. Comparison of ground signatures of C25D-P extracted from USM3D viscous simulations. Propagated near-field ground signatures extracted at 3 body lengths away from C25D. M_∞=1.6, α=0.0º, Rn=5.7 million per meter.
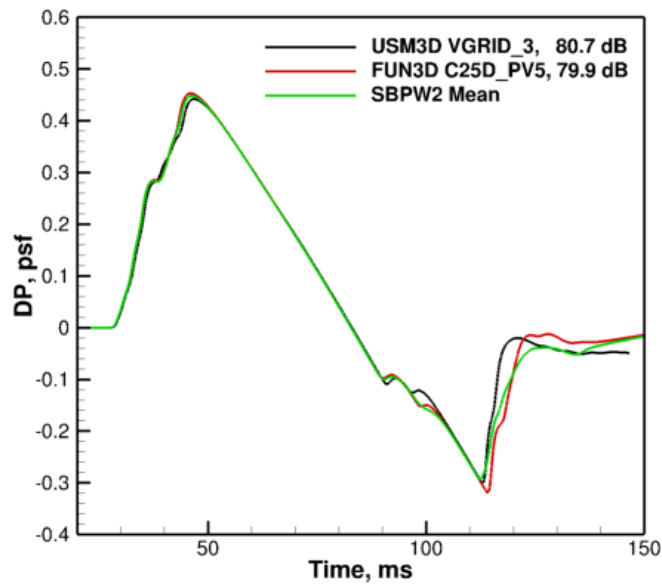

Figure 22. Comparison of ground signatures at H/L=3. for the C25D-P. M_∞=1.6, α=0.0º, Rn=5.7 million per meter.

American Institute of Aeronautics and Astronautics